A Haptic Probe for Soft Tissue Abnormality Identification during Minimally Invasive Surgery

Hongbin Liu[1], Oussama Elhage[2], Prokar Dasgupta[2], Ben Challacombe[3], Declan Murphy[2], Lakmal Seneviratne[1], Kaspar Althoefer[1]

[1]Department of Mechanical Engineering, Kings College London
Strand, London, WC2R 2LS, United Kingdom
Hongbin.liu@kcl.ac.uk
lakmal.seneviratne@kcl.ac.uk
kaspar.althoefer@kcl.ac.uk

[2] Department of Urology, Guy's and St Thomas' Hospital
Great Maze Pond, London, SE1 9RT, United Kingdom
oelhage@yahoo.com
prokarurol@gmail.com
decmurphy@doctors.net.uk

[3] Department of Urology, Royal Melbourne Hospital
Grattan Street, Melbourne,VIC 3050, Australia
benchallacombe@doctors.org.uk

Abstract—*This paper proposes a novel haptic probe for the identification of tissue properties during minimally invasive surgery (MIS). The purpose of such a device is to compensate a surgeon for a portion of the loss of haptic and tactile feedback experienced during robotic-assisted MIS. A prototype for validating the concept in an ex-vivo setting was developed and used to characterize two different testing modalities - rolling tissue indentation and uniaxial tissue indentation. A MIS compatible design (capable of passing through 10mm hole) is also presented. The key feature of the wheeled device is the ability to measure the tool-tissue interaction force as well as the rolling indentation depth concurrently. The purpose of the rolling indentation is to generate a mechanical image which can indicate tissue abnormalities, such as tumors, which are difficult to isolate under static testing conditions. After locating the abnormal region, the uniaxial indentation is subsequently conducted on the region of interests for detailed investigation. Experiments on a silicone phantom show that the developed prototype is capable of rapidly locating embedded hard nodules within the silicone model. Moreover by performing static additional uniaxial indentation, the device can be used to identify the parameters of the tissue viscoelastic constitutive equation.*

Index Terms—*Haptics, Soft tissue identification, Minimally invasive surgery*

1. INTRODUCTION

Advances in robotic-assisted minimally invasive surgery (MIS) introduce many benefits into conventional MIS. The most well known robotic surgical is the da Vinci™ Surgical System (Intuitive Surgical, Inc. [1]. Distinct advantages of this system include high distal dexterity, enhanced 3D vision, motion scaling, tremor filtering and direct hand-eye coordination eliminating reversed tool motions. These advances result in improved ergonomics and also allow complex surgical procedures, which are usually difficult to be conducted by conventional minimally invasive means such as coronary artery bypass grafting [2] and mitral valve repair [3], to be effectively performed. However, the lack of haptic feedback in the current robotic systems is still one of the major downsides of the surgical systems. For instance, in robotic urological procedures, the lack of haptic feedback can cause problems during surgery, especially when attempting to remove cancer such as locally advanced T3 prostate cancer and large bulky muscle invasive bladder cancer.

The aim of this paper is to introduce a new haptic probe which can rapidly identify the stiffness distribution of an investigated soft tissue to facilitate the localization of the tissue abnormalities, compensating the loss of haptic feedback commonly associated with MIS. Our method is using the haptic probe to roll over a large area of an organ during MIS and concurrently measure the tool-tissue interaction force as well as the rolling indentation depth information. The force signals and the indentation depth signals collected from the device can be used to calculate the stiffness of the underlying soft tissue along the rolling path. By fusing the tissue stiffness along the rolling path, the tissue geometrical stiffness distribution can be mapped in form of a pseudo-colour image. As a malignant tumour will typically be stiffer than the surrounding normal tissue [4], hence it allows a surgeon to rapidly identify abnormal tissue regions via checking high stiffness area on the image. To characterise the soft tissue mechanical properties in detail, uni-axial indentations are applied on the identified abnormal regions, and the constitutive equation of those regions can be determined by using experimental data.

Haptics, which represents the sensation felt by the human hand, is a term to describe both force (kinaesthetic) information and tactile (cutaneous) information [5]. Using tactile feedback to measure the tissue-instrument interaction for tissue diagnosis has been proposed by numerous researches. The use of a transrectal probe equipped with tactile sensors to identify prostate tumours was described in [6]. Tactile feedback systems have also been proposed for identification and characterization of pulmonary tumours [7], lesions in the breast [8] and for identifying arteries during robotic surgery [9]. While the results from above works demonstrate that tactile feedback systems have potential as tissue diagnostic tools, their adaptation to the MIS is less than ideal due to the problems associated with cost, miniaturisation and sterilisation.

Measuring force feedback from tissue-instrument interaction for tissue diagnosis has also been widely studied. A computerized endoscopic surgical grasper which can measure mechanical properties of the grasped tissue is described in [10]. By applying automated palpation, the grasper can distinguish between lung, spleen, liver, colon, intestine and stomach. In [11], a strain gauge-sensorized laparoscopic grasper was developed to detect the compliance of the object via measuring the grasping force and grasper position. In [12], the feasibility of utilizing a force-sensitive probe to localize lung tumours based on tissue stiffness variations is discussed. The above works show that using kinaesthetic feedback for tissue diagnosis during MIS is an approach with good potential.

The primary novelty of the rolling indentation is that instead of performing a series of discrete uni-axial measurements, the wheel allows for the continuous measurement of the underlying mechanical response of the tissue as it rolls over the surface of an organ. This allows for rapid coverage of a surface and enhanced sensitivity to tissue irregularities. As only a force/torque sensor and positioning system are required, the adaptation of the wheel rolling indentation into robotic MIS is promising.

2. The Prototype of The Haptic Probe

To conduct a lab-based feasibility study, a prototype of the haptic probe was constructed as shown in Fig 1. The entire unit is attached to the distal tip of a Mitsubishi RV-6SL 6-DoF (degree of freedom) robotic manipulator to allow for accurate motion control. The device consists of two separate sensing components, each equipped with a wheel as end-effector. The first wheel, Wheel-A, measures the rolling wheel-tissue interaction force, and the second wheel, Wheel-B, measures the corresponding rolling indentation depth.

The force sensing component is used for sensing the interaction force imparted on the wheel during rolling indentation. An ATI NANO17 Force/Torque sensor (SI-12-0.12 with 16-bit DAQ (NI PCI 6034E)) is connected directly with the Wheel-A. This allows for the measurement of the three force components (Fx, Fy, Fz) imparted by the tissue onto the wheel. Wheel-A is a plastic wheel which has diameter 8mm and width 8mm. The wheel was grooved with 12 teeth along its circumference to avoid slip during rolling and mounted in a miniature ball bearing to minimize frictional losses.

The indentation depth sensing component consists of a fiber-optic displacement sensor and a spherical end-effector (Wheel-B in Fig.2) with 5 mm in diameter. The principle of the displacement sensing probe is based on 'bent optic fiber pair configuration'. It consists of a LED light source, emitting/reflecting unit and an optical detecting circuit [13]. Data from both the Force/Torque sensor and the displacement sensor are acquired using the National Instruments LabView 8.0 software package and associated PCI Data Acquisition Cards.

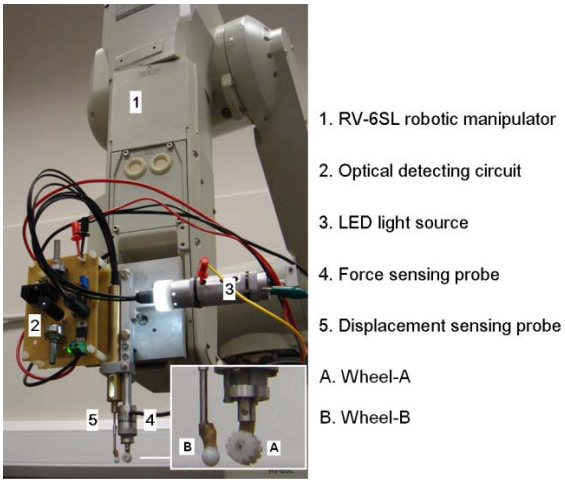

Fig.1. The prototype of the haptic device for the soft tissue abnormality identification

3. The Principle of the Measurement of the Wheel Indentation Depth

All paragraphs must be indented. All paragraphs must be justified, i.e. both left-justified and right-justified. An intra-operative vision based technique to infer wheel indentation depth could have been alternatively used, however the mechanical device to directly measure the relative distance between the wheeled probe and surrounding tissue was found to be a more practical solution. As shown in Fig. 1, Wheel-A is connected directly to the force sensor and Wheel-B is connected with the sliding rod of the displacement sensor. Wheel-B has an unconstrained range of movement of 8mm along the vertical axis and contact between it and the underlying tissue is maintained only by gravity.

The principle of the measurement of the wheel indentation depth is that, when Wheel-A indents into the soft tissue under control from the robot manipulator, Wheel-B will not indent, but rather will be pushed upwards by the surrounding tissue as the indentation depth increases, Fig.2.

According to experimental observation, the soft tissue deformation in the vicinity of the Wheel-A follows an exponential curve as shown in Fig. 2. Hence, even if the Wheel-B is placed slightly away from the Wheel-A in the *x*

direction, the differential distance (H_d) along z axis between the Wheel-A and the Wheel-B is very similar to actual indentation depth (H_t). The tissue deformation curve can be assumed as:

$$H_d = H_t(1 - e^{\lambda x}) \quad (1)$$

where H_t is the true indentation depth of Wheel-A, H_d is the differential distance between Wheel-A and Wheel-B along z axis, when Wheel-B is l mm away from Wheel-A along x axis. Laboratory calibration shows the parameter λ in the tissue deformation curve is -0.275 for silicone.

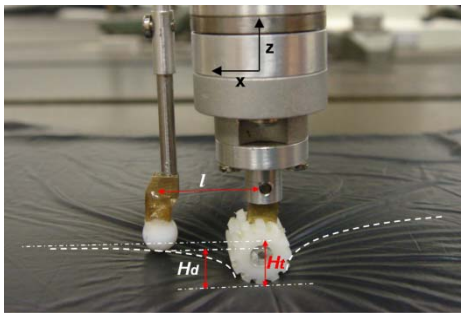

Fig.2. The principle of the measurement of the wheel indentation depth

The displacement sensing probe is used to measure the differential distance H_d between Wheel-A and Wheel-B. To avoid the collision between the two wheels, Wheel-B was placed away from Wheel-A by 12mm in this paper.

To investigate the accuracy of the wheeled indentation depth sensor, a series of validation tests were conducted on a homogenous silicone block as shown in Fig.3. Nine paths which are 90 mm along x axis with 9 mm shift in y axis were defined as the rolling path for the probe. During the validation experiment, the probe was rolled over the silicone block along the predefined paths with various indentation depths. The changing of the indentation depth was controlled by the robotic manipulator through varying the z axis coordinate of the rolling paths. The indentation depths during rolling indentation were measured by the indentation depth sensor and compared with the known ground truth data to analysis the error introduced by the indentation depth sensor.

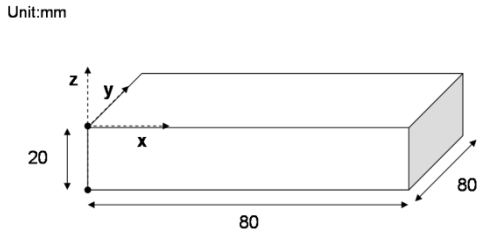

Fig.3. The homogenous silicone block used for the validation of the indentation depth sensor.

The results demonstrate that when the indentation depth is greater than 3mm, the percentage error of the measurement is less than 10% (resolution ≈ 0.2mm) and the wheeled indentation depth sensor can be used to accurately measure the rolling indentation depth. As shown in Fig.4, the error is high for small indentation depth. This is due to the nonlinearity of the fibre optic displacement sensor, as the sensor has low sensitive for small indentation depth and high sensitivity for large indentation depth.

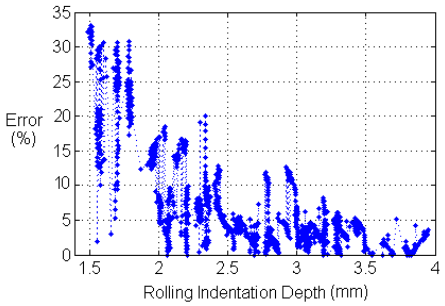

Fig.4. The percentage error of the indentation depth measurement along the increase of the rolling indentation depth.

4. Depth Rolling Indentation Modality

The prime function of the wheeled probe is the rapid inspection of tissue abnormalities for a large area of the testing sample by applying rolling indentation modality. The purpose of the rolling indentation is to examine the changes in tissue reaction force while the wheel rolls over the tissue sample. An abnormality may manifest itself as an abrupt peak or a high plateau which is beyond the threshold of normal tissue. By applying the rolling indentation technique to cover a large area and generate a stiffness map, the relevant spatial changes of tissue stiffness can be inspected thoroughly and the abnormal region within the soft tissue can be identified. The results presented in this section describe the rolling indentation tests on silicone phantom to develop the stiffness map as well as link the map with the known ground truth data from the phantom internal structure.

Natural soft tissue has complicated internal structures with large amount of arteries or veins making it extremely difficult to acquire the internal configuration of a tissue sample for comparison to the measured mechanical image under laboratory conditions. Therefore a silicone phantom suitable for soft tissue simulation (RTV6166, General Electric [14]) with six simulated rubber nodules was constructed. The dimensions of the phantom and the nodules are shown in Fig. 5. The main mechanical properties of the silicone and rubber are listed in Table I.

To generate the stiffness distribution map of the internal structure of the silicone model a series of 50 paths parallel to the x axis were defined, with a shift of 2mm along the y axis between paths. The force imparted by the sample onto the wheel, as measured by the Force/Torque sensor, and the rolling indentation depth, as measured by the indentation depth sensor were recorded during each traverse.

To obtain the map of the stiffness distribution of the silicone phantom, the first step was to convert the force signal to stress data and convert the rolling indentation depth to compressive strain data. The force signal was converted to the stress using $\sigma = f/A$, where σ is the stress, f is the tissue reaction force and A is the contact area between the wheel and tissue. To simplify the problem, during the rolling indentation using Wheel-A, the contact area was assumed 8×8 mm^2 as the Wheel-A is 8mm in width and 8mm in diameter.

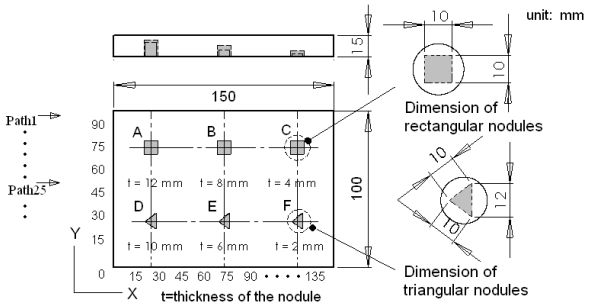

Fig. 5. The dimension of the silicone phantom displaying location, shape and depth of the six simulated nodules (A-F), each with a thickness, *'t'*

TABLE I
MECHANICAL PARAMETERS OF THE SILICONE PHANTOM

	Elastic Modulus (Pa)	Poisson's Ratio	Shear Modulus (Pa)	Mass Density (kg/m^3)
Rubber	8.7x10^6	0.49	2.9x10^6	1000
Silicone	4.9x10^5	0.45	1.63x10^5	4980

The rolling indentation depth was converted to the compressive strain using $\varepsilon = H_t / h$, where the ε is the compressive strain, H_t is the rolling indentation depth, h is the high of the silicone, i.e. h = 15 mm. From the experimental observation, it was found that the stress-strain function of the silicone can be governed by the Neo-Hookean model. Therefore the stiffness of the silicone can be calculated using the strain and stress data as:

$$\mu = \sigma / (\varepsilon^2 + \varepsilon^{-1}), \qquad (2)$$

where the μ represents the tissue stiffness, ε is the strain and σ is the stress. By processing the stress and strain data using Eq.2, The stiffness data can be obtained.

As shown in Fig. 6, these stiffness data along the roll path were then stitched together to generate a stiffness image using *Matlab*^{TM}. The image projects the geometry of stiffness distribution of the rolling area into an x-y plane. This procedure was conducted for rolling indentation depths of 4mm.

In order to measure the accuracy of nodules locating, the image was analyzed using the *Matlab Image Processing Toolbox*. Fig. 6 shows that nodules A, B, D are clearly visible and their locations on the rolling image are consistent with their counterparts in the silicone phantom. Table II lists the relative errors of locations of the centroid of the visible nodules between on the physical model and the rolling mechanical image.

These results show that the stiffness map can be used for identify the location of abnormalities buried inside a simulated soft tissue sample. This is particularly applicable to the field of robot-assisted minimally invasive surgery (MIS) as it could potentially be used to allow a surgeon probe a solid organ intra-operatively.

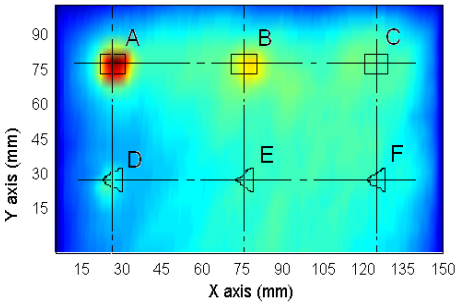

Fig. 6. The rolling mechanical images from the silicone phantom with embedded nodules

TABLE II
THE LOCATIONS OF THE CENTROID OF VISIBLE NODULES

Nodules	Location at Silicone (x, y)	Location at the image (x, y)	|Relative Error
NoduleA	(25.0, 75.0)	(22.2, 74.1)	(11.2%, 1.2%)
NoduleB	(75.0, 75.0)	(72.6, 76.1)	(3.0%, 1.5%)
NoduleD	(25.0, 25.0)	(24.5, 22.7)	(2.0%, 9.2%)

5. UNIAXIAL INDENTATION MODALITY

5.1. Purpose of Uniaxial Indentation and Mathematic Modelling

The stiffness map generated from rolling indentation modality indicates the location of tissue abnormality through preliminarily examining changes in tissue stiffness while the wheel rolls over the tissue sample. To thoroughly identify the viscoelastic properties of abnormal tissue regions, addition uniaxial indentation tests are requested to perform on peculiar areas.

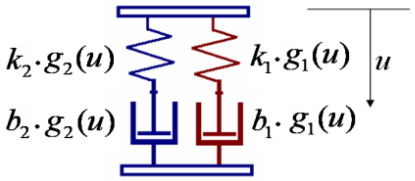

Fig.7. Dual Maxwell Model with nonlinear functions

To analyze measurements from uniaxial indentation and thus extract the viscoelastic properties of the tissue samples, a mathematic viscoelastic tissue model is demanded working in conjunction with static indentation tests. The authors'

previous work [15, 16] has shown that by adding nonlinear functions into a linear dual Maxwell model, the nonlinear viscoelastic characteristics of tissue samples can be simulated accurately and comprehensively, when modelling parameters are properly calibrated.

The proposed model is as shown in Fig. 7, two nonlinear functions ($g_1(u)$, $g_2(u)$), are added to each linear Maxwell Model. These nonlinear functions are used to account for both shallow and large deformations. u is the tissue deflection (indentation depth, unit in meter), k_i, b_i ($i=1,2$) are the elastic modulus and material coefficient of viscosity respectively. The Constitutive Equation of this nonlinear model was derived as the following equation:

$$f+(\frac{b_1}{k_1}+\frac{b_2}{k_2})\dot{f}+\frac{b_1b_2}{k_1k_2}\ddot{f}=[g_1(u)b_1+g_2(u)b_2]\dot{u}+[g_1(u)\frac{b_1b_2}{k_2}+g_2(u)\frac{b_1b_2}{k_1}]\ddot{u} \quad (3)$$

where f is the reaction force when the model is subjected a deflection u. $g_1(u)=1+g_{12}u+g_{13}u^2$, $g_2(u)=1+g_{22}u+g_{23}u^2$, g_{12}, g_{13}, g_{22}, g_{23} are the polynomial coefficients.

5.2. Uniaxial Indentation Results

To further analyze the viscoelastic properties of the highlighted areas (A, B, D) in Fig. 6, a set of uniaxial indentation tests were carried out on particular areas. For each area, the Wheel-A was indented into the tissue with a fixed indentation depth and held steady for 10 seconds to record the stress relaxation curve. The indentation depth varied from 1 to 6 mm with 1mm increments.

The experimental results were modeled and analyzed using the dual Maxwell model. The tissue mechanical properties of the above selected areas were analyzed in two aspects: 1) the force-tissue deflection function and 2) modeling parameters for tissue viscoelastic properties. Table III shows the list of modeling parameters of tissue nonlinear viscoelasticity calibrated at different testing areas.

TABLE III
MODELING PARAMETERS OF TISSUE VISCOELASTICITY CALIBRATED AT DIFFERENT TESTING AREAS

	A	B	D
k_1(n/m)	0.043	5.67	1.63
k_2 (n/m)	0.11	14.18	4.08
b_1(n.s/m)	0.012	1.48	0.48
b_2(n.s/m)	1.56	175.8	63.09
g_{12} (*10^5)	6.04	0	0
g_{13} (*10^5)	6.06	0	0
g_{22} (*10^8)	3.81	0.016	0.037
g_{23} (*10^8)	3.77	0.018	0.038

It can be seen from the analysis results that as tissue has heterogenous viscoelastic properties associated with different testing locations, it is necessary to first perform rolling indentation to identify the abnormal tissue region before conducting more detailed investigation on tissue mechanical properties.

6. MIS-COMPATIBLE WHEELED PROBE

The above experimental study of the functionality of the prototype proposed in this paper have proven that the feasibility of such a device for rapid conducting diagnosis to locate tissue abnormalities. However to be utilized in MIS surgery, it is compulsory to miniaturize the wheeled device.

Based the concept of the initial prototype design, the MIS compatible wheeled device will be redesigned and manufactured to allow the access through a strand Trocar port of 10mm in diameter(see Fig.8). The future wheeled device will be fully applied with fiber-optical sensing scheme and the use of non-electronics component would allow the device capable of enduring the clinical sterilization procedure.

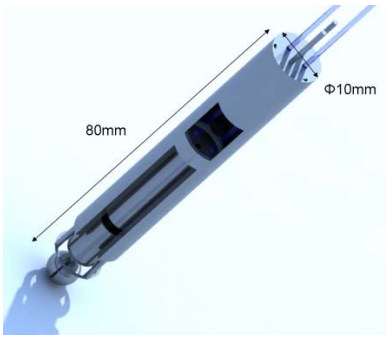

Fig.8. The future MIS-compatible wheeled probe

As shown in Fig. 9, the main components of the future device include a fiber-optic force sensor (1) attached with a wheel end-effector (3), and a fiber-optic displacement sensor consist of a sliding mechanism (2) attached with a reflector (9) and a ring (4). (7), (8) are the transmitting fiber, receiving fiber for the force sensor, and (5), (6) are the transmitting fiber, receiving fiber for the displacement sensor.

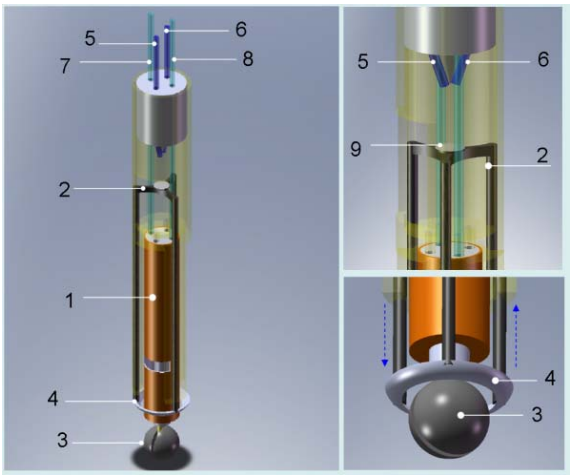

Fig.9. The structure/ components of the MIS-compatible wheeled device

Comparing with the prototype, the modification for the future device involves two main aspects:

Force Sensor –the commercial Nano17 sensor (17mm in diameter) is replaced by a cylindrical fibre-optic force sensor. The force sensor is 6mm in diameter, proportionally scaled down from the 10mm-diameter prototype developed in authors' previous work [13].

Displacement Sensor–the fiber-optic displacement sensor is miniaturized down to 10mm in diameter and arranged in series with the force sensor. The cylindrical Wheel-A (8mm in diameter, 8mm in width) is changed to a spherical wheel with 6mm in diameter. The Wheel-B is transformed from the cylindrical wheel to a ring connecting with the sliding mechanism. The transmitting/receiving fibers of the force sensor and the ones of the displacement sensor are arranged in an equal space, with avoiding the contact with the sliding mechanism.

REFERENCES

[1] G. S. Guthart, and J. K. Salisbury Jr., "The IntuitiveTM telesurgery system: Overview and application", in Proc. IEEE Int. Conf. Robotics and Automation, pp. 618-621, 2000.

[2] H. A. Tabaie, J. A. Reinbolt, W. P. Graper, T. F. Kelly, and M. A. Connor, "Endoscopic coronary artery bypass graft (ECABG) procedure with robotic assistance", The Heart Surgery Forum, vol. 2, no. 4, pp. 310-317, 1999.

[3] D. A. Murphy, J. S. Miller, D. A. Langford, and A. B. Snyder, "Endoscopic robotic mitral valve surgery", J. Thorac. Cardiovasc. Surg., vol. 132, no. 4, pp. 776-781, Oct. 2006.

[4] J. D. Brown, J Rosen, Y.S. Kim, et al., In vivo and in situ compressive properties of porcine abdominal soft tissues, In Medicine Meets Virtual Reality II, Westwood JD, Hoffman HM, Mogel GT, et al.(eds). IOS Press: Amsterdam, The Netherlands, pp.26–32. 2003.

[5] A. M. Okamura, Methods for Haptic Feedback in Teleoperated Robot-Assisted Surgery. Industrial Robot, An International Journal, 31(6):499-508. 2004

[6] V Egorov, S Ayrapetyan, AP Sarvazyan (2006) Prostate Mechanical Imaging: 3-D Image Composition and Feature Calculations, IEEE Trans. Med. Imag., 25(10):1329-1340.

[7] A. P. Miller, WJ Peine, JS Son, *et al*. Tactile imaging system for localizing lung nodules during video-assisted thoracoscopic surgery. In Proc. IEEE Int. Conf. Robot. Autom., Rome, Italy, 2996–3001. 2007.

[8] S. P. Wellman (2001) Tactile Imaging of Breast Masses: First Clinical Report, *Arch Surg.* 136:204-208

[9] R. A. Beasley, RD Howe. Tactile tracking of arteries in robotic surgery. In Proc. IEEE Int. Conf. Robot. Autom., Washington, DC, 2002; 4: 3801–3806.

[10] B Hannaford, J Trujillo, M Sinanan, *et al*. Computerized endoscopic surgical grasper. In *Medicine Meets Virtual Reality*, Westwood JD, Hoffman HM, Stredney D, *et al*. (eds). IOS Press: Amsterdam, The Netherlands, 1998; 265–271.

[11] A Bicchi, G Canepa, D De Rossi, et al., A sensor-based minimally invasive surgery tool for detecting tissue elastic properties, In IEEE Int. Conf. Robot. Autom., Minneapolis, MN, USA; 1996; 1: 884–888.

[12] G. L. McCreery, A. L. Trejos, M. D. Naish, R. V. Patel, R. A. Malthaner, "Feasibility of locating tumours in lung via kinaesthetic feedback",Int. J. Med. Robotics Comput. Assist. Surg., vol. 4, pp.58-68, Mar. 2008.

[13] P. Puangmali, H. Liu, K. Althoefer, and L. D. Seneviratne, "Optical Fiber Sensor for Soft Tissue Investigation during Minimally Invasive Surgery", in Proc. IEEE Int. Conf. Robot. Autom., 2008, pp. 2934-2939

[14] A. M. Okamura, C. Simone, and M.D. O'Leary, "Force Modelling for Needle Insertion into Soft Tissue," IEEE Transactions on Biomedical Engineering, Vol. 51, No. 10, pp. 1707-1716, 2004

[15] D. Noonan, H. Liu, Y. Zweiri, K. Althoefer, L. D. Seneviratne, "A dual-function wheeled probe for tissue viscoelastic property identification during minimally invasive surgery", in Proc. IEEE Int. Conf. Robot. Autom., Rome, Italy, Apr. 2007, pp.2629-2634.

[16] H Liu, DP Noonan, YH Zweiri, K Althoefer, LD Seneviratne, The Development of Nonlinear Viscoelastic Model for the Application of Soft Tissue Identification, IEEE/RSJ Int. Conf. Intelligent Robots and Systems, 208-213,2007